Dalton Transactions

Accepted Manuscript

ROYAL SOCIETY OF CHEMISTRY

www.rsc.org/dalton

Journal Name

ARTICLE

Linear Coordination Polymers Based on Aluminum Phosphates: Synthesis, Crystal Structure and Morphology

Received 00th January 20xx,
Accepted 00th January 20xx

DOI: 10.1039/x0xx00000x

www.rsc.org/

M. Dębowski,* K. Łokaj, A. Wolak, K. Żurawski, A. Plichta, J. Zachara, A. Ostrowski and Z. Florjańczyk*

Several aluminum tris(diorganophosphates) have been synthesized and characterized via elemental analysis, NMR, FT-IR and Raman spectroscopies, as well as powder XRD, and SEM. Single-crystal X-ray diffraction studies revealed that aluminum tris(diethylphosphate) crystal structure comprises two crystallographically nonequivalent *catena*-Al[$O_2P(OEt)_2$]$_3$ chains propagating along the *c*–axis. Their parallel orientation favors the formation of closely packed hexagonal domains. PXRD data suggest that other homologues have a similar structure, with the interchain distance closely corresponding to the dimensions of organic ligands. They are also susceptible to a reversible dissociation to ionic species under the effect of primary amines. This feature can be utilized for the synthesis of epoxy nanocomposites.

Introduction

The phosphate group is one of the essential components of a variety of biological macromolecules and synthetic materials. Considerable effort has been devoted to the development of synthetic analogues of nucleic acids, lipids and enzymes, as well as the mimicking of some processes that occur in living organisms,[1–4] for example, selective cation transport in liquid membrane systems[1,5–7] and biomineralization.[8–10] Esters of phosphoric acid are often used as starting materials in the synthesis of coordination polymers formed by metal cations linked by organic ligands, molecular clusters, or hybrid inorganic-organic mesostructured lamellar systems.[11–20] Some of these hybrid materials, as well as their analogues with phosphonate groups, are considered promising candidates for a variety of practical applications, e.g. organogelators, flame retardants, fillers in polymer composites, processable precursors of mesoporous zeolites, and thin films with high abrasion resistance and low refractive index.[21–36]

An important class of these materials consists of organically modified aluminum phosphates synthesized from mono- or diesters of phosphoric acids and various sources of aluminum cations. The reaction of phosphoric acid monoesters with aluminum inorganic salts or trialkoxides has been successfully applied in the synthesis of two-dimensional plate-like particles consisting of aluminum phosphate phases separated by long organic chains,[16,18,19] as well as nanosize octameric and decameric clusters that can serve as building blocks for framework structures.[37] It has been observed that dimers [$R_2AlO_2P(OR')_2$]$_2$ or tetramers [$(RO)_2AlO_2P(OR')_2$]$_4$ were formed when phosphoric acid diesters are reacted with equimolar amounts of trialkylaluminum[27,38] or trialkoxyaluminum,[27] respectively. Furthermore, chemical transformation of these cyclic oligomers allows for the fabrication of aluminophosphate materials,[27] silicoaluminum phosphates,[39,40] and 2D framework solids.[41]

We have previously explored the use of boehmite and diphenylphosphoric acid (DPhP)[38] or triethyl phosphate (TEP)[42–45] for the preparation of spherical nanoparticles that consist of aluminum oxohydroxide cores covered by a layer of organically modified aluminum phosphates. These products were shown to improve certain mechanical properties of polymer composites based on polyurethane,[45] or carboxylated styrene-butadiene rubber.[42,46] We have also observed that, in such systems, increasing the reaction time favors the formation of highly crystalline fibers composed of hexagonally packed *catena*-Al[$O_2P(OR)_2$]$_3$ chains (R = Et[45], Ph[38]). It has been suggested that these fibers are formed via the self-assembly of aluminum cations and $(RO)_2PO_2^-$ anions in solution.[45] This type of hybrid material may be of practical interest because the mechanical reinforcement gained from fibers is significantly higher than that gained from spherical fillers.[47] Some recent publications suggest also that the presence of Al[$O_2P(OR)_2$]$_3$ nanorods can affect other properties of the polymer matrix, for example enhancing orientation in liquid-crystalline epoxy resins cured in an external magnetic field.[48,49]

To expand our knowledge of this class of coordination polymers, we decided to investigate in detail their structural and morphological properties, as well as the way they are influenced by the synthetic procedures and the type of organic

[a] *Faculty of Chemistry, Warsaw University of Technology, Noakowskiego 3, 00-664 Warsaw, Poland.*
† E-mail (Dębowski): debowski@ch.pw.edu.pl; E-mail (Florjańczyk): evala@ch.pw.edu.pl.
†Electronic Supplementary Information (ESI) available: SEM images of DPhPAl, FT-IR and Raman spectra of DOPAl samples, additional crystal structure details including CIF, tabulated PXRD data for DOPAl samples, NMR spectral data. CCDC 1404032. See DOI: 10.1039/x0xx00000x

groups present in the phosphate moiety. In view of those objectives we developed effective methods for the synthesis of pure aluminum tris(diorganophosphate) (DOPAl) utilizing different sources of aluminum. We examined the physicochemical and morphological properties of the resulting materials using single-crystal or powder XRD studies, ^{27}Al and ^{31}P NMR, Raman or FT-IR spectroscopies, as well as SEM technique. In this paper, we report the synthesis and characterization of coordination polymers with the general formula $Al[O_2P(OR)_2]_3$ containing alkyl groups [R= Me (DMPAl), Et (DEPAl), ^{n}Pr (DnPPAl), ^{i}Pr (DiPPAl), ^{n}Bu (DBPAl), $CH_2CH(Et)(CH_2)_3CH_3$ (BEHPAl) or phenyl moieties [R= Ph (DPhPAl)] in aluminum phosphate monomeric units.

Experimental

Materials and characterization methods

All chemicals for syntheses were purchased from commercial sources and were used without further purification: trimethyl phosphate (TMP) (97%, Aldrich), TEP (99%, Aldrich), tri-*n*-propyl phosphate (TnPP) (99%, Aldrich), triisopropyl phosphate (TiPP) (99%, Aldrich), tri-*n*-butyl phosphate (TBP) (97%, Aldrich), triphenyl phosphate (TPhP) (99%, Merck Chemicals), di-*n*-butyl phosphate (DBP) (97%, Aldrich), bis(2-ethylhexyl) phosphate (BEHP) (97%, Aldrich), DPhP (99%, Aldrich), aluminum L-lactate (AlLact) (97%, Aldrich), triethylaluminum (TEA) (1.9 M solution in toluene, Aldrich), sodium bicarbonate (pure, POCh Gliwice). Toluene used in the reactions involving TEA was distilled from sodium-benzophenone ketyl solution and stored over dry 4 Å molecular sieves under nitrogen atmosphere.

The hydrogen and carbon contents were determined using a Perkin-Elmer CHNS/O II 2400 instrument. Powder X-ray diffraction (PXRD) patterns were recorded at room temperature on a Seifert HZG-4 automated diffractometer using Cu-Kα radiation (λ = 0.15418 nm). The data were collected in the Bragg-Brentano (θ/2θ) horizontal geometry (flat reflection mode) between 4° and 60° (2θ) in 0.04° steps at 10 s/step. In the case of DnPPAl, the TOPAS software[50] (Bruker AXS) was utilized for indexing the PXRD pattern using 22 reflections (2θ < 38°), as well as Pawley refinement of the obtained cell parameters. ^{1}H, ^{27}Al and ^{31}P NMR spectra were recorded in solution on a Varian 400 MHz spectrometer operating at 400.11, 104.25, and 161.96 MHz, respectively. Chemical shifts are reported relative to external standards: TMS (^{1}H), $[Al(H_2O)_6]^{3+}$ (^{27}Al), and 85% $H_3PO_{4(aq)}$ (^{31}P). Solid-state ^{27}Al MAS NMR measurements were performed on a Bruker DSX 300 spectrometer at a spinning rate of 6–8 kHz with proton high-power decoupling and a resonance frequency of 78.20 MHz. Solid-state ^{31}P CP/MAS NMR measurements were conducted on a Bruker DSX 300 spectrometer at a spinning rate of 5–8 kHz, resonance frequency of 121.50 MHz and contact time of 1–1.5 ms. FT-IR spectra were recorded on a Thermo Scientific Nicolet 6700 spectrometer equipped with a Smart Orbit Diamond ATR accessory. Raman spectra were collected on a Thermo Nicolet Almega XR spectrometer equipped with 532-nm laser. The particle size distribution in the studied dispersions was determined using a dynamic light scattering (DLS) method. The measurements were conducted on a Malvern Zetasizer Nano ZS instrument equipped with 532-nm laser. SEM images were obtained on a Zeiss LEO 1530 field emission scanning electron microscope equipped with a GEMINI column. Before the measurements, all samples were coated with an electron conductive layer of carbon utilizing a high-vacuum carbon sputter coater.

Single-crystal structure analysis

A single crystal of DEPAl was selected under a polarizing microscope and mounted in inert oil (Immersion Oil type A, Cargill) and transferred to the cold gas stream of the diffractometer. Diffraction data were measured at −173(2) °C using graphite-monochromated Mo-Kα radiation on an Oxford Diffraction κ-CCD Gemini A Ultra diffractometer. Cell refinement and data collection, as well as data reduction and analysis, were performed with the Oxford Diffraction software program CrysAlisPRO.[51] The structure was solved and refined in SHELXL-97.[52] Crystal data and the details of structure determinations are given in Table 1. A more detailed description of structure determination as well as some selected bond distances and bond angles (Tables S1–S5) are given in Electronic Supplementary Information. Crystallographic data for the structure reported in this paper have been deposited in the Cambridge Crystallographic Data Center with CCDC number 1404032.

Preparation of DOPAl samples

Reactions of AlLact with Phosphoric Acid Triester (TOP). Method M1: In the case of water-miscible TMP or TEP, DOPAl was synthesized according to the following procedure: AlLact (6.0 g, 20 mmol) was dissolved in redistilled water (20 mL) followed by the addition of TOP (60 mmol). The mixture was heated under reflux (48 h), during which a white solid material precipitated. The crude product was isolated via filtration on a Schott funnel and purified by washing with water and then methanol. The final product was obtained after drying at 70–80 °C under an air flow. In this manner, DMPAl (7.5 g, 94%) and DEPAl (8.8 g, 92%) were synthesized.

Method M2: All reactions of AlLact with TOP containing hydrophobic alkyl chains (C_3, C_4, and C_8) or phenyl groups required temperatures in the range of 130–150 °C and the use of pressure vessels. A typical synthesis was performed as follows: AlLact (3.0 g, 10 mmol) was dissolved in redistilled water (20 mL) followed by the addition of TOP (30 mmol). The mixture was placed in a stainless steel or thick-walled glass pressure reactor and heated in an oil bath (24 h). After cooling to room temperature, the crude product was isolated via filtration on a Schott funnel and purified by washing with water and an organic solvent (methanol in the case of DnPPAl, DiPPAl, and DBPAl or acetone in the case of DPhPAl). The final product was obtained after drying at 70–80 °C under an air flow. In this manner, DnPPAl (1.4 g, 25%), DiPPAl (3.9 g, 70%), DBPAl (3.9 g, 60%) or DPhPAl (1.4 g, 18%) were synthesized.

Method M3: The procedure was identical to that described in the case of Method M2, but the reaction was performed in a mixture of water and 1,4-dioxane (1:1 v/v). In this manner, DPhPAl (3.3 g, 43%) was obtained.

Reactions of AlLact with Phosphoric Acid Diester (DOP).

Method M1: A typical synthesis proceeded according to the following procedure: AlLact (3.0 g, 10 mmol) was dissolved in redistilled water (20 mL) followed by the addition of DOP (30 mmol). The mixture was vigorously stirred at room temperature (15 min), during which a solid precipitated. The insoluble product was isolated via filtration on a Schott funnel and purified by washing with water and methanol. The final product was obtained after drying at 70–80 °C under an air flow. In this manner, DBPAl (6.4 g, 98%) was synthesized.

Method M2: The procedure was very similar to Method M1, but the reaction mixture was heated under reflux (24 h). In this manner, BEHPAl (7.4 g, 75%) was synthesized (the crude insoluble product was washed with acetone).

Method M3: The procedure was identical to that described previously (see TOP synthetic route, Method M2) with the exception that DOP was used as the phosphorus source. In this manner, DPhPAl (6.9 g, 90% after 1h of heating and 6.8 g, 89% after 24h of heating) could be synthesized.

Reactions of AlLact with Phosphoric Acid Diester Sodium Salt (DOPNa). A typical synthesis was performed in 2 steps. First, DOP (30 mmol) was neutralized with a 10 wt% aqueous solution of sodium bicarbonate (2.520 g, 30 mmol). A solution of AlLact (3.0 g, 10 mmol) in water (10 g) was added dropwise under vigorous stirring to the resulting clear solution of DOPNa. Even at room temperature, the ion-exchange reaction proceeded very quickly. Depending on the type of organic ligand used, an insoluble product (DOPAl) precipitated (in the case of DBPAl and DPhPAl) or formed a stable dispersion (in the case of BEHPAl); BEHPAl could be isolated by salting out with NaCl. The crude DOPAl was isolated and purified according to the previously described procedures (see DOP synthetic route). In this manner, DBPAl (5.8 g, 90%), BEHPAl (9.1 g, 93%) or DPhPAl (3.5 g, 45%) were synthesized.

Reactions of TEA with DOP. All operations were performed in a purified nitrogen atmosphere. A solution of DBP (6.501 g, 30 mmol) in toluene (10 mL) was added dropwise to a vigorously stirred mixture of TEA (5.3 mL, 10 mmol) and toluene (10 mL) that was precooled to −70 °C. The reaction mixture was allowed to warm up to room temperature for 1 h. Stirring was continued at that temperature for an additional 12 h, resulting in the formation of an opalescent, viscous liquid or gel. After completion of the reaction, all volatiles were removed under reduced pressure, yielding DBPAl (5.6 g, 86%) as a white solid. Using BEHP (9.972 g, 30 mmol) in place of DBP and stirring the reaction mixture under reflux (12 h), BEHPAl (9.7 g, 98%) was obtained.

Unless stated otherwise the analytical, spectroscopic or X-ray diffraction data presented in this paper for DBPAl refer to the sample obtained from TEA and DBP (see DOP-TEA synthetic route), whereas in the case of BEHPAl or DPhPAl such data relate to the products prepared from the respective DOPNa (see DOPNa synthetic route).

$Al[O_2P(OMe)_2]_3$ (DMPAl). Found: C, 18.18; H, 4.65%. Calc. for $C_6H_{18}AlO_{12}P_3$: C, 17.92, H 4.51%. FT-IR (neat, cm^{-1}): 2983(w), 2957(w), 2851(w), 1463(w), 1448(w), 1219(m), 1190(m), 1134(m), 1085(w), 1068(w), 1034(s). 837(s), 792(w), 778(w), 632(w), 544(m), 523(s), 494(s), 479(s). Raman (neat, cm^{-1}): 3018(m), 3000(m), 2968(s), 2863(w), 1472(w), 1198(w), 1059(w), 855(w), 789(m), 589(m). ^{27}Al MAS NMR δ(78 MHz): −27.3 ppm. ^{31}P MAS NMR δ(121 MHz): −7.7 and −10.4 ppm, integral ratio 16.59:10.00. ^{1}H NMR δ(saturated solution, 400 MHz, D_2O): 3.75 (d, J = 11.4 Hz), 3.67 ppm (dd, J = 11.1, 1.7 Hz), 3.58 ppm (dd, J = 10.7, 1.6 Hz), integral ratio 1.00:4.03:6.60. ^{1}H NMR δ(dilute solution, 400 MHz, D_2O): 3.77 (dd, J = 11.0, 2.4 Hz), 3.68 ppm (dd, J = 11.1, 1.4 Hz), 3.59 ppm (d, J = 10.7 Hz), integral ratio 1.00:11.25:26.82. ^{31}P NMR δ(saturated solution, 162 MHz, D_2O): 5.82 (s), −3.47 (s), and −8.79 ppm (s), integral ratio 10.17:6.09:1.00. ^{31}P NMR δ(dilute solution, 162 MHz, D_2O): 5.87 (s) and −3.43 ppm (s), integral ratio 2.50:1.00. ^{27}Al NMR δ(dilute solution, 104.25 MHz, D_2O): −1.16, −2.44, and −5.88 ppm.

$Al[O_2P(OEt)_2]_3$ (DEPAl). Found: C, 29.89; H 6.13%. Calc. for $C_{12}H_{30}AlO_{12}P_3$: C, 29.64; H, 6.22%. FT-IR (neat, cm^{-1}): 2981(w), 2933(w), 2905(w), 2868(w), 1483(w), 1438(w), 1397(w), 1366(w), 1220(m), 1201(w), 1135(s), 1071(m), 1035(s), 972(s), 962(s), 819(m), 782(m), 621(w), 557(m), 505(m), 474(m). Raman (neat, cm^{-1}): 2983(m), 2942(s), 2909(m), 2870(w), 2787(w), 2730(w), 1454(w), 1294(w), 1106(w), 1047(w), 794(w), 552(w). ^{27}Al MAS NMR δ(78 MHz): −14.9 and −21.3 ppm. ^{31}P MAS NMR δ(121 MHz): −14.7 ppm.

$Al[O_2P(O^nPr)_2]_3$ (DnPPAl). Found: C, 37.92; H, 7.48%. Calc. for $C_{18}H_{42}AlO_{12}P_3$: C, 37.90; H 7.42%. FT-IR (neat, cm^{-1}): 2965(w), 2937(w), 2877(w), 1464(w), 1378(w), 1214(m), 1136(s), 1062(s), 997(s), 906(w), 886(w), 868(m), 845(w), 749(m), 567(m), 520(m), 473(m). Raman (neat, cm^{-1}): 2983(w), 2943(w), 2889(w). ^{27}Al MAS NMR δ(78 MHz): −26.0 ppm. ^{31}P MAS NMR δ(121 MHz): −16.8 ppm.

$Al[O_2P(O^iPr)_2]_3$ (DiPPAl). Found: C, 37.95; H, 7.44%. Calc. for $C_{18}H_{42}AlO_{12}P_3$: C, 37.90; H, 7.42%. FT-IR (neat, cm^{-1}): 2977(w), 2919(w), 2866(w), 1456(w), 1384(w), 1373(w), 1237(m), 1154(m), 1096(m), 1018(m), 992(s), 898(w), 789(m), 624(w), 556(w), 528(m), 463(m). Raman (neat, cm^{-1}): 2988(m), 2931(s), 2878(m), 2741(w), 1461(w), 1371(w), 1226(w), 1123(w), 756(w). ^{27}Al MAS NMR (78 MHz): δ −28.2 ppm. ^{31}P MAS NMR δ(121 MHz): −9.3 and −21.5 ppm, integral ratio 1.00:96.57.

$Al[O_2P(O^nBu)_2]_3$ (DBPAl). The results of elemental analysis are presented in Table 2. FT-IR (neat, cm^{-1}): 2956(m), 2932(w), 2906(w), 2872(w), 1465(w), 1429(w), 1379(w), 1217(s), 1137(s), 1064(s), 1025(s), 984(s), 911(m), 850(w), 811(w), 734(w), 624(w), 573(m), 523(w), 478(s). Raman (neat, cm^{-1}): 2972(m), 2945(s), 2920(s), 2883(s), 2739(w), 1462(w), 1310(w), 1134(w), 915(w), 844(w). ^{27}Al MAS NMR δ(78 MHz): −24.0 ppm. ^{31}P MAS NMR δ(121 MHz): −16.9 ppm. ^{27}Al NMR of sample prepared according to TOP synthetic route δ(104 MHz, 1:2 v/v mixture of $CDCl_3$ and hexan-1-amine): 0–10 ppm (signal overlapping with artificial probe signal). ^{31}P NMR of sample prepared according to TOP synthetic route δ(162 MHz, 1:2 v/v mixture of $CDCl_3$ and hexan-1-amine): −0.52 ppm.

$Al[O_2P(OCH_2CH(Et)(CH_2)_3CH_3)_2]_3$ (BEHPAl). The results of elemental analysis are presented in Table 2. FT-IR (neat, cm^{-1}): 2934(s), 2928(m), 2872(m), 2861(m), 1462(m), 1379(w), 1204(m), 1133(s), 1063(s), 1028(s), 884(m), 767(w), 726(w), 622(m), 563(m), 479(s). Raman (neat, cm^{-1}): 2934(s), 2896(s), 2873(s), 2730(w), 1449(w), 1297(w), 1143(w), 1053(w). ^{27}Al MAS NMR δ(78 MHz) (overlapping signals): −18.6 and −30.7 ppm (highest intensity). ^{31}P MAS NMR δ(121 MHz) (overlapping signals): −0.1, −3.3, −4.4, and −13.4 ppm (highest intensity). ^{27}Al NMR of sample prepared according to DOP synthetic route δ(104 MHz, $CDCl_3$): −20 to 10 ppm (broad and overlapping signals). ^{27}Al NMR of sample prepared according to DOP synthetic route δ(104 MHz, C_6D_6): −17.72 ppm (broad peak with a downfield shoulder). ^{27}Al NMR of sample prepared according to DOP synthetic route δ(104 MHz, CD_3OD): −4.60 and −15.32 ppm (broad and overlapping signals). ^{31}P NMR of sample prepared according to DOP synthetic route δ(162 MHz, $CDCl_3$) (broad and overlapping signals): −2.14, −2.88, −6.41, −13.33, −15.00, and −17.80 ppm. ^{31}P NMR of sample prepared according to DOP synthetic route δ(162 MHz, C_6D_6) (broad and overlapping signals): −0.80, −6.14, −12.07, −12.92, −14.46, and −17.26 ppm. ^{31}P NMR of sample prepared according to DOP synthetic route δ(162 MHz, CD_3OD): 3.15, −0.10, −1.63, −3.48, −11.89, and −15.22 ppm.

$Al[O_2P(OPh)_2]_3$ (DPhPAl). The results of elemental analysis are presented in Table 2. FT-IR (neat, cm^{-1}): 3063(vw), 1590(m), 1488(m), 1456(w), 1288(w), 1228(m), 1202(s), 1121(s), 1071(m), 1026(m), 1006(m), 944(s), 901(w), 772(s), 749(s), 686(s), 628(w), 561(s), 499(s), 468(s). Raman (neat, cm^{-1}): 3191(vw), 3069(s), 1601(w), 1239(w), 1167(w), 1037(w), 1015(m), 951(w), 742(w), 625(w). ^{27}Al MAS NMR of sample prepared according to DOP synthetic route, Method M3 δ(78 MHz): −22.5 ppm. ^{31}P MAS NMR of sample prepared according to DOP synthetic route, Method M3 δ(121 MHz): −26.1 ppm (unsymmetrical, with shoulder to high-field region).

Results and discussion

Synthesis and morphology of DOPAl

TOP Synthetic Route. The major route for synthesizing DOPAl applied in the present study involved reactions of phosphoric acid triester (TOP) with AlLact (Scheme 1a). These reactions were performed in water at temperatures between 100 and 150 °C, depending on the type of TOP used. In the case of water-miscible TMP or TEP, a simple heating of the reaction mixture under reflux resulted in the formation of DMPAl or DEPAl in yields exceeding 90%. Under these conditions, TOP underwent gradual hydrolysis, yielding the respective diester of phosphoric acid (DOP), which subsequently reacted with the aluminum substrate.[45]

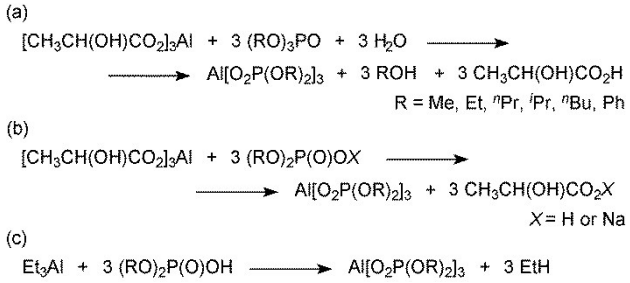

Scheme 1. General synthetic routes to DOPAl applied in this paper: (a) TOP route, (b) DOP or DOPNa route, and (c) DOP-TEA route.

Initially, these reactions were performed in solution, and after approximately 4 h, a white solid consisting of DOPAl began to precipitate; the amount of solid increased with time. SEM images revealed that the products formed fibrous particles with particle diameters in the range of 0.1–2.0 µm (Fig. 1A). The particles were placed irregularly and formed irregular unwoven fabrics. We also observed that, under suitable conditions (T = 130 °C and pressure of approximately 1.5 MPa), DEPAl could be synthesized in the form of large (approximately 100 µm in diameter) crystals that are suitable for X-ray structure determination.

All syntheses involving TOP containing hydrophobic alkyl chains or phenyl groups required temperatures in the range of 130–150 °C and the use of pressure vessels. Under such conditions pure DOPAl were obtained in yields between 20 and 70%. The morphology of DOPAl containing ^{n}Pr or ^{i}Pr groups was very similar to that of DMPAl or DEPAl, as indicated by SEM images (an example in Fig. 1B for DnPPAl). Particles with much more regular shapes were easily obtained when TBP or TPhP were utilized. The compounds DBPAl and DPhPAl formed rod-like structures with cross-sections similar to a regular hexagon and diameters of 0.2–2.0 µm (Fig. 1C for DBPAl). In contrast, BEHPAl exhibited a wax-like consistency.

DOP, DOPNa, and DOP-TEA synthetic routes. DOPAl can be synthesized directly from an appropriate amount of DOP or its sodium salt (DOPNa). The aluminum source can be AlLact (Scheme 1b) or TEA (Scheme 1c). In our studies, these methods were tested using *n*-butyl, 2-ethylhexyl, or phenyl derivatives. The reactions of AlLact with DBP or its sodium salt were performed at room temperature, using water as the solvent. After mixing the solutions of both reagents, DBPAl almost immediately precipitated. DBPAl synthesized in this manner formed large, irregular agglomerates composed of spherical particles with diameters of 0.5–1.0 µm (Fig. 1D). Due to the higher hydrophobicity of BEHP, its reaction with AlLact required prolonged heating under reflux. Under these conditions, a wax-like solid of BEHPAl was separated from the mixture, and its amount increased over time; after 24 h, the overall yield was 75%. The morphology of this product (Fig. 1E) was very similar to that of DBPAl synthesized via an analogous process. BEHP neutralization with an aqueous solution of sodium bicarbonate followed by the slow addition of an AlLact solution led to the formation of a stable dispersion containing particles with an average size of approximately 200 nm. BEHPAl could be precipitated from this system via salting out

with a saturated NaCl solution. SEM analysis of the resulting product (Fig. 1F) indicated that it consisted mainly of irregular agglomerates. However, there was also a small fraction of rod-like domains.

Despite its lack of solubility in water, DPhP easily yielded the desired product when heated to 130 °C in an aqueous solution of AlLact. Even after 1 h, rod-like particles of DPhPAl (Fig. S1A–S1B, ESI†) could be obtained almost quantitatively. However, increasing the reaction time resulted in the formation of crystallites with more regular and uniform shapes. These crystallites measured a few micrometers long and exhibited hexagonal cross-sections with diameters less than 1 μm (Fig. S1C–S1D, ESI†). Samples of DPhPAl with very similar morphologies could be obtained at lower temperatures and over shorter reaction times when the sodium salt of DPhP was used (Fig. S1E–S1F, ESI†).

The reactions of DOP with TEA were performed according to a modified procedure described in our previous paper.[38] They resulted in the formation of the appropriate DOPAl in nearly quantitative yield. In SEM images of the as-synthesized compounds BEHPAl (Fig. 2A) or DBPAl (Fig. 2B), one cannot distinguish any submicron rod-like particles. The large structures present in these samples possessed an irregular (DBPAl) or continuous surface (BEHPAl). Heating DBPAl in toluene led to very small changes in sample morphology, e.g., a slight increase in the porosity of the particle surface (Fig. 2C). However, replacing toluene with a mixture of 1-butanol and water (40:60 v/v) and heating to 130 °C induced the formation of 2D nanoparticles (Fig. 2D) similar in shape to those obtained from AlLact and TBP.

It should be noted that the carbon or hydrogen contents in DOPAl samples prepared by different chemical routes but containing the same organic ligands are in good agreement with those calculated for the respective aluminium tris(diorganophosphates) (Table 2). This strongly indicates that the choice of the method of preparation only affects DOPAl morphology, with no changes in the chemical composition of the resulting product.

Crystal Structure of DEPAl at −173 °C

One of the main objectives of our studies was to obtain DOPAl in a form suitable for single-crystal X-ray analysis. We anticipated that the solving its structure could provide us the reference data required to properly characterize other organically modified aluminum phosphates using powder XRD. We managed to synthesize such a material via the TEP and AlLact reaction performed in a dilute system under hydrothermal conditions (130 °C, 1.5 MPa). The obtained DEPAl crystals were subjected to a reliable single-crystal X-ray analysis at −173 °C.

DEPAl crystallizes into a trigonal crystallographic system, space group $P\overline{3}$ and forms a linear coordination polymer propagating along the *c*–axis of its unit cell (Fig. 3). In its structure, one can distinguish two crystallographically nonequivalent chains that are characterized by a 3-fold symmetry axis parallel to the [001] direction. The symmetries of those structures can be described by $p\overline{3}$ and $p3$ rod groups, respectively. The chains propagating along the edges of the DEPAl unit cell, where aluminum atoms are also located at inversion centers, belong to the former group and are hereafter referred to as *A*-type chains. The chains exhibiting lower symmetry (*B*-type chains) are situated within the unit cell (Fig. S2, ESI†).

The collected crystallographic data indicate that both types of DEPAl chains show considerable similarities in structure when considering the coordination spheres of aluminum and phosphorus. The chains are formed by the linking of the adjacent aluminum centers by three O–P–O bridges, each of which belongs to a different phosphate group. The plane of the O–P–O bridge is inclined at an angle of 22.7° with respect to the *c*–axis, which creates the potential for a change in the Al...Al distance due to temperature or interactions between chains.

The Al–O distances vary between 1.8803(7) and 1.8917(12) Å. The cis O–Al–O angles are in the range of 88.65(4)–91.35(4)°, whereas angles between O ligands in trans positions differ from 180° by less than 0.2°. The lengths of the P–O bonds vary between 1.4944(8) and 1.5843(11) Å, whereas the O–P–O angles range from 101.37(5) to 118.82(4)° (Tables S2–S3, ESI†). The coordination numbers of aluminum and phosphorus in each type of DEPAl chain are equal to 6 and 4, respectively. All P and Al centers are surrounded by oxygen ligands located at the vertices of the corresponding polyhedra. Each PO_4 tetrahedron shares two of its O atoms with two AlO_6 octahedra.

The calculated distortion of the AlO_6 octahedron (Δ_{Al}), the O–Al–O angle variances (σ^2), the aluminum bond valence sums (s_{Al}),[53] and the length of the resultant bond-valence vector ($|\mathbf{v}_{Al}|$) for each crystallographically independent aluminum atom are summarized in Table 3. The Δ_{Al} values can be estimated by the modified general equation (Eq. (1)) that was successfully applied in the case of TiO_6 octahedra in titanates.[54]

$$\Delta_{Al} = 6^{-1} \times \sum_i [(d_i - d_{ave})/d_{ave}]^2 \quad (1)$$

where d_i and d_{ave} represent the interatomic distances of Al–O and the average value, respectively.

To estimate the strains at phosphorus centers, one can apply the bond-valence vector (BVV) model proposed by Zachara.[55] Table 4 contains data regarding the length of the resultant bond-valence vector ($|\mathbf{v}_P|$) for each crystallographically independent phosphorus center in the DEPAl structure.

As shown Δ_{Al}, the σ^2 and $|\mathbf{v}_{Al}|$ values are very low, which indicates that the octahedral environments of the oxygen ligands around all of the aluminum metal centers remain nearly undistorted. Furthermore, the bond valence sums calculated for each type of Al center are close to 3, the theoretically expected value for trivalent elements. In contrast, in the case of the PO_4 group, the deviation of its geometry from that of a regular tetrahedron is significant. Generally, the P–O bonds involved in the bridging of aluminum atoms are on average 5% shorter than those involved in connecting alkyl groups. In contrast, the angles between them, which approach 120°, are 12–15% greater than those between ester linkages. The largest constraints on the geometry of the coordination

sphere were estimated for the phosphorus centers in the *B*-type DEPAl chains, for which the resultant bond-valence vectors were the longest (Table 4). These vectors are directed outwards from the chain and obliquely to the symmetry axis (Fig. S3, ESI†), which indicates that the largest strains are caused by the arrangement of the organic ligands. It should also be noted that, according to the BVV model, the smallest strains occur in the phosphate tetrahedra forming *A*-type chains for which the value of $|\mathbf{v}_P|$ is almost equal to 0.

The main structural difference between *A*-type and *B*-type DEPAl chains is the conformation of the ethyl groups around the phosphorus centers. In *A*-type chains, all P atoms are crystallographically equivalent, and the O–P–O–C torsion angles characterizing each of the organic substituents connected to them are equal to 65.57(8) and 69.26(8)° (Table S4, ESI†). In agreement with IUPAC recommendations,[56] these ethyl groups have a *gauche–gauche* (G^+G^+) conformation. In contrast, the chains with lower symmetry (*B*-type chains) contain two crystallographically unequal phosphorus centers, each of which is characterized by a *gauche–trans* arrangement of alkyl groups (G^-T and G^+T for the P11 and P12 centers, respectively). Based on the theoretical calculations performed for dimethylphosphate anions, the *gauche–gauche* conformation is thermodynamically more stable than the *gauche–trans* one.[57]

A detailed analysis revealed that the periodicity of each DEPAl chain is equal to the *c*–axis vector, and there are no directional interactions, e.g., hydrogen bonds, beyond van der Waals packing contacts. Each polymer chain is surrounded by six others, where the aluminum centers are shifted alternately in the *c*–axis direction by +1/6 and −1/6 of its vector value (Fig. S4, ESI†). As a result, the DEPAl structure is characterized by hexagonal close-packing.

Powder XRD patterns of DOPAl samples

Fig. 4 shows a simulation of the DEPAl powder XRD pattern calculated based on the data collected by single-crystal X-ray analysis and the results of PXRD measurements performed at room temperature. As shown, at −173 °C, the largest diffraction peak occurs at 2θ = 8.65°. This peak is attributed to the diffraction of X-rays on the (2−10) lattice plane, which is perpendicular to the *a*–axis and passes through the aluminum metal centers of one *A*-type and one *B*-type DEPAl chain. The interplanar distance characterizing this plane (d_{2-10} spacing) is equal to 10.22 Å. It is worth noting that, with increasing temperature, the main XRD reflection did not disappear but shifted to lower value of 2θ, suggesting that DEPAl retained its hexagonally packed structure and the d_{2-10} spacing increased. However, one cannot exclude a certain degree of translational movement of the DEPAl chains in the *c*–axis direction.

The analysis of PXRD diffractograms obtained for other DOPAl samples (Fig. 5 and Tables S6–S13, ESI†) allows for the hypothesis that they may form crystal structures analogous to the structure of DEPAl with polymeric chains arranged in a hexagonal close-packing pattern. This behavior is suggested by the similarities in the shapes of the respective PXRD patterns, particularly the presence of a single, high-intensity diffraction peak at low values of 2θ. These reflections most likely arise from the diffraction phenomena occurring on the lattice planes parallel to the axis of the DOPAl chain and passing through its aluminum centers – the exact analogues of the DEPAl (2−10) plane. We tried to carry out a full-profile refinement of the cell parameters of different DOPAl complexes, for example by applying Pawley fitting. Unfortunately, for a majority of DOPAl samples such calculations gave unreliable results due to an insufficient number of reflexes observed, especially in the area of low values of 2θ. The only exception occurred in the case of DnPPAl (Fig. S5, ESI†), for which we obtained the following cell parameters: a = 23.6800(11) Å, c = 9.2316(10) Å, and cell volume of 4475.4(7) Å^3 (space group $P\bar{3}$), consistent with the model of DOPAl structure proposed by us. In order to verify our hypothesis about the similarities in crystal structures formed by different aluminium tris(diorganophosphates) we decided to try another approach. By assuming that the average Al...Al distance in each DOPAl chain is constant and equal to approximately 4.6 Å, one can evaluate the volume attributable to a single monomeric unit in $Al[O_2P(OR)_2]_3$ crystals (V_{XRD}) based on the position of the highest, low-angle reflex observed on the DOPAl PXRD patterns. These values can also be calculated using empirical relationships between the volume of each structural unit and the unit's arrangement in space (V_{calcd}).[58] The results obtained using both methods are summarized in Table 5.

As shown, both methods yield very similar values for the monomeric unit volume with differences of only a few percent. It should be noted that in the case of DnPPAl the same situation occurs, if we compare its V_{XRD} value with that evaluated based on the cell volume obtained from Pawley fitting of the PXRD pattern and the assumption that Z parameter is equal to 6 (V_{Pawley} = 746 Å^3). This good agreement between the values of V_{XRD} and V_{calcd} (or V_{Pawley}) supports the initial hypothesis that DEPAl and other DOPAl compounds possess analogous hexagonal close-packed polymeric structures, where the distance between chains depends on the dimensions of the organic ligands.

Solid-state MAS NMR spectra of DOPAl

The ^{27}Al MAS NMR spectra of the majority of the DOPAl samples recorded at room temperature show a single, broad resonance peak with a maximum located between −21 and −31 ppm (Fig. 6). The observed peak positions are consistent with the literature data previously reported for aluminum centers in AlO_6 octahedra forming crystalline structures of aluminum methylphosphonates[59–62] and natural or synthetic hydrated aluminum phosphates.[63,64] The broadening of the signal most likely arises from the high quadrupole moments and electric field gradients of aluminum nuclei, suggesting that lower symmetry effectively reduces the spin-lattice relaxation time. However, one cannot exclude that the presence of aluminum centers in non-equivalent crystallographic environments may also contribute to the line shape.

Similarly, the ^{31}P MAS NMR spectra of the majority of the DOPAl samples exhibit only one symmetric signal at δ between

−10 and −26 ppm, depending on the type of organic ligand used (Fig. 6). The spectral feature suggests that there is only one type of phosphorus chemical environment, which can be attributed to the tetrahedral phosphorus nuclei in aluminum phosphates.[18,65,66] In contrast, the ^{31}P MAS NMR spectra of DMPAl or BEHPAl show several signals from non-equivalent phosphorus nuclei, whose precise origin remains unclear.

FT-IR and Raman spectra of DOPAl

Based on the literature data concerning the FT-IR and Raman spectra of ammonium,[67] sodium[57] or barium[68] dialkyl phosphates, as well as those obtained from theoretical studies on the vibrational spectra of dimethyl[57,67,69] or diethyl[68] phosphate anions, one can expect four diagnostic bands associated with the stretching modes of phosphate ligands to appear over the wavenumber range of 750–1250 cm^{-1}. Analogously to previous assignments, we suggest that the two strong bands observed in the FT-IR spectra of DOPAl samples between 1115–1140 and 1190–1230 cm^{-1} (Fig. S6–S9, ESI†) can be attributed to the symmetric and asymmetric stretching vibrations of P–O bonds in Al–O–P–O–Al bridges, respectively.[57,68] The asymmetric stretching mode is prominent only in the FT-IR spectra, whereas the corresponding symmetric mode is also active in the Raman spectra (Fig. S6, ESI†). However, the position of the latter is not exactly the same as that in the FT-IR spectra, most likely due to contributions from the symmetric C–O stretching mode. The absorption bands attributable to the symmetric O–P–O stretching mode of the phosphodiester group in DOPAl occur in the range of 750–790 cm^{-1} in both the infrared and Raman spectra.[57,68] The Raman intensities of these signals are significantly greater than those of the symmetric P–O stretching bands in the bridging units. The corresponding asymmetric mode gives rise to IR bands in the range of 820–850 cm^{-1},[57,68] which can also be observed as weak signals or shoulders in the Raman spectra of DOPAl.

The characteristic absorption bands for O–Al–O vibrations in bridging units are most likely located between 480 and 620 cm^{-1}. In the FT-IR spectra of the investigated DOPAl, one can distinguish 5 highly intense signals in this region. However, these signals may overlap with weak bands that are attributable to the deformation modes of phosphate moiety.

The other stretching and bending modes of C–H, C–C, or C–O bonds give rise to several additional bands with wavenumbers between 900 and 3000 cm^{-1}. However, these bands are not of immediate interest in this study.

It is worth noting that the FTIR spectra of BEHPAl, DPhPAl or DBPAl samples obtained in different chemical reactions are almost identical (Figures S7, S8 or S9 in ESI†, respectively). This observation, in combination with the results of elemental analysis (see Table 2), suggests that for a given organic group in the phosphate moiety the use of different synthetic routes results in the formation of the same DOPAl complex.

DOPAl in solution

DOPAl compounds are insoluble in aprotic organic solvents and even the presence of large hydrocarbon ligands merely results in the formation of a stable colloid dispersion, as in the case of BEHPAl mixed with benzene, hexane, chloroform, diethyl ether or THF. Based on the NMR studies of those systems, one can assume that the particles are stabilized by a small fraction of soluble aluminum phosphate species. The signals observed in the ^{27}Al NMR spectra of BEHPAl (Fig. S10, ESI†) are broad and often overlap the artificial probe signal located at δ≈ 50 ppm. Nevertheless, in a spectrum recorded in C_6D_6, one can distinguish a distinct asymmetric resonance peak with a chemical shift (−17.7 ppm) close to that detected in the MAS NMR measurements, which suggests the presence of polymeric species structurally similar to the particles in the solid sample. In contrast, the corresponding ^{31}P NMR spectra of BEHPAl (Fig. S10, ESI†) show at least four different signals at δ values between −20 and 10 ppm, depending on the choice of solvent. This indicates that, in solution, diorganophosphate ligands can coordinate aluminum centers in various ways.

One of the most important features of DOPAl is its ability to form true solutions in primary amines. We hypothesize that, in these systems, DOPAl undergoes dissociation to diorganophosphate anions and complex aluminum cations, as indicated in Eq. (2). This conclusion is supported by the results of the NMR studies of the DBPAl/hexan-1-amine model system (Fig. S11, ESI†).

$$Al[O_2P(OR)_2]_3 + 6\,R'NH_2 \longrightarrow [Al(R'NH_2)_6]^{3+} + 3\,[(RO)_2PO_2]^- \quad (2)$$

The ^{27}Al (Fig. S11a, ESI†) and ^{31}P (Fig. S11b, ESI†) NMR spectra of DBPAl in a $CDCl_3$/hexan-1-amine mixture (1:2 v/v) do not exhibit any signals at chemical shifts typical of polymeric DOPAl species. Instead, the phosphorus resonance spectrum shows a single peak at a δ value of approximately 0 ppm, which is also present in an analogous spectrum recorded for the hexan-1-amine salt of DBP (Fig. S11c, ESI†). ^{27}Al NMR measurements revealed that the resonance signals of the aluminum cations are not clearly visible and only account for a broadening of the probe signal at approximately 0 ppm.

It is worth noting that amine-induced dissociation of DOPAl is a reversible process. For example, a polymeric form of DBPAl can again be obtained as a precipitate if the saturated solution prepared at room temperature from 16 g of DBPAl and 100 g of hexan-1-amine is cooled to 4 °C. The same applies to the case in which amine is consumed in a chemical reaction and can be utilized for the preparation of polymer nanocomposites. We examined this approach by curing an epoxy resin with a DPhPAl solution in triethylenetetramine, which led to the formation of small nanoparticles dispersed in a solid matrix (Fig. 7). The resulting polymer composites exhibit reduced flammability and some improvements in their mechanical properties.[42,70]

Among all of the DOPAl species we synthesized, only those containing methyl or ethyl groups exhibited very limited solubility in water, approximately 0.4–0.5 g per 100 g of H_2O at room temperature. The ^{27}Al and ^{31}P NMR studies of DMPAl solutions in D_2O (Figures S12 and S13 in ESI†, respectively) revealed the presence of several populations of phosphorus or

aluminum nuclei, each of which existed in a different chemical environment. The signal positions for the aluminum species are reasonable for aluminum cations complexed by water (δ value of approximately 1.2 ppm) or aluminum cations exhibiting a mixed surrounding of water and dimethylphosphate ligands (broad and overlapping signals with δ values of approximately −2.3 and −5.9 ppm).[71,72] The sharp peak observed in the ^{31}P NMR spectrum at a δ value of 5.8 ppm is most likely related to the free $[(CH_3O)_2PO_2]^-$ ions, whereas the additional low-intensity signals located between 0 and −10 ppm arise from the same ligands complexing aluminum centers.[71,72] The relative intensity of the latter decreases with increasing dilution of the DMPAl solution. The presence of several different dimethylphosphate species is also confirmed by the shape of the ^{1}H NMR spectrum (Fig. S14, ESI†), in which one can distinguish three groups of signals related to protons of methoxy groups. These species are characterized by chemical shifts of approximately 3.58, 3.67 and 3.75 ppm. A careful analysis of the relative integral intensities of ^{1}H and ^{31}P NMR signals and their dependence on the DMPAl solution concentration suggest that the farthest upfield signal in the ^{1}H NMR spectra is related to the free dimethylphosphate anions. The two other resonance peaks that decreased with dilution most likely arose from dimethylphosphate species coordinating aluminum centers. It is worth noting that, even in a concentrated DMPAl aqueous solution, approximately 57% of the dimethylphosphate groups existed as free ions (Table 6). It is also interesting that, after the evaporation of water from such systems, one can recover the DMPAl coordination polymer. Therefore, it can be assumed that, during synthesis, the morphology of each DMPAl particle is constantly changing and depends on the balance between dissolution and precipitation. This behavior is supported by the fact that the solubility of DMPAl in water at the boiling point of the reaction mixture is approximately 22 times higher than that estimated at room temperature.

Our studies indicate that, over a given period (24 h), diorganophosphate moieties in DMPAl or DEPAl are hydrolytically stable at temperatures of up to approximately 100 °C. However, in the case of the methyl derivative, an increase in temperature results in gradual hydrolysis of P–OR linkages. We observed that an insoluble product precipitated from aqueous solutions of DMPAl heated for 1 h at 150 °C. The FT-IR spectrum of this solid (Fig. S15, ESI†) does not contain absorption bands characteristic of the C–H stretching modes that, in an analogous DMPAl spectrum, show maxima at 2957 and 2851 cm^{-1}. Instead, one can distinguish two very strong bands at wavenumbers of 3359 and 3177 cm^{-1} attributable to the O–H stretching modes of hydroxyl groups formed during the hydrolysis of phosphoester linkages. Substantial differences also occur with respect to the MAS NMR spectra (Fig. S16, ESI†). The insoluble product of DMPAl hydrolysis is characterized by two resonance peaks of ^{31}P nuclei located at −23.80 and −29.23 ppm that can be attributed to PO_4^{3-} ligands in partially hydrated aluminum phosphate. A corresponding ^{27}Al MAS NMR spectrum exhibits several signals within the ranges of chemical shifts typical of tetrahedral and octahedral aluminum centers in $AlPO_4$.[66]

Based on the results of studies performed on DEPAl, DBPAl, and BEHPAl, one can conclude that these compounds have a high chemical resistance to concentrated solutions of strong mineral (HCl, HNO_3, H_3PO_4, H_2SO_4) or organic (acetic, trichloroacetic, p-toluenesulfonic) acids, even when heated to 50 °C for 24 h. However, they easily transform into aluminum hydroxide when treated with 10 or 20 wt% solutions of NaOH in water or ethanol.

Conclusions

We have shown that aluminum tris(diorganophosphates) form *catena*-$Al[O_2P(OR)_2]_3$ polymeric chains, which parallel location favors the formation of closely packed hexagonal crystalline domains. Both the type of organic group R and the method of preparation strongly affect the morphology of the product. Therefor one can obtain DOPAl samples containing highly crystalline fibers with hexagonal cross-sections, irregular agglomerates or amorphous wax-like phases.

DOPAl species are insoluble in aprotic organic solvents or strong inorganic acids. Only BEHPAl forms solutions or stable colloidal dispersions in selected organic media. DOPAl containing methyl or ethyl groups are sparingly soluble in water, in which they act as dynamers susceptible to changes in the solution concentration. Similarly, under the effects of primary amines, samples of DOPAl undergo a reversible dissociation to ionic species and form true solutions that can be successfully applied as curing systems for epoxy resins.

It is worth noting that DOPAl samples exhibit very interesting thermal properties that are the subject of the ongoing studies and will be discussed in detail in a separate paper.

Acknowledgements

This research was partially funded through the Structural Funds in the Operational Programme - Innovative Economy (IE OP) financed from the European Regional Development Fund - Project "Modern material technologies in aerospace industry", No. POIG.01.01.02-00-015/08-00.

Notes and references

1 S. Penczek and P. Klosinski, in *Biomimetic Polymers*, ed. C. G. Gebelein, Plenum Press, New York, 1990, chapter 12, 223–241.
2 S. Penczek and P. Klosinski, in *Models of Biopolymers By Ring-Opening Polymerization*, ed. S. Penczek, CRC Press, Inc., Boca Raton, FL, 1989, chapter 4, 291–378.
3 A. Eschenmoser, *Chimia*, 2005, *59*, 836.
4 S. Penczek, J. Pretula and K. Kaluzynski, *Biomacromolecules*, 2005, **6**, 547.
5 R. Wódzki and P. Kłosiński, *Macromol. Chem.*, 1990, **191**, 921.
6 R. Wódzki, M. Świątkowski and G. Łapienis, *React. Funct. Polym.*, 2005, **62**, 195.
7 R. Wódzki, M. Świątkowski and G. Łapienis, *React. Funct. Polym.*, 2010, **70**, 463.

8 K. Kaluzynski, J. Pretula, G. Lapienis, M. Basko, Z. Bartczak, A. Dworak and S. Penczek, *J. Polym. Sci., Part A: Polym. Chem.*, 2001, **39**, 955.
9 J. Rudloff, M. Antonietti, H. Cölfen, J. Pretula, K. Kaluzynski, S. Penczek, *Macromol. Chem. Phys.*, 2002, **203**, 627.
10 S. Penczek, J. Pretula and K. Kaluzynski, *J. Polym. Sci., Part A: Polym. Chem.*, 2005, **43**, 650.
11 V. G. Lebedev, K. K. Palkina, S. I. Maksimova, E. N. Lebedeva and O. V. Galaktionova, *Zh. Neorg. Khim.*, 1982, **27**, 2980.
12 Y. Han, Z. Pan, N. Shi, L. Liao, C. Liu, G. Wu, Z. Tang and Y. Xiao, *Wuji Huaxue Xuebao*, 1990, **6**, 17.
13 C. G. Lugmair, T. D. Tilley and A. L. Rheingold, *Chem. Mater.*, 1997, **9**, 339.
14 M. Fröba and M. Tiemann, *Chem. Mater.*, 1998, **10**, 3475.
15 M. Fröba and M. Tiemann, *Chem. Mater.*, 2001, **13**, 3211.
16 H. Tanaka and M. Chikazawa, *J. Mater. Chem.*, 1999, **9**, 2923.
17 H. Tanaka and M. Chikazawa, *Mater. Res. Bull.*, 2000, **35**, 75.
18 M. Schulz, M. Tiemann, M. Fröba and C. Jäger, *J. Phys. Chem. B*, 2000, **104**, 10473.
19 Y. Huang and Y. Zhimin, *J. Am. Chem. Soc.*, 2005, **127**, 2731.
20 T. Kimura, *Microporous Mesoporous Mater.*, 2005, **77**, 97.
21 A. Vioux, J. Le Bideau, P. H. Mutin, D. Leclercq, *Top. Curr. Chem.*, 2004, **232**, 145.
22 ed. A. Clearfield, K. Demadis, *Metal Phosphonate Chemistry: From Synthesis to Applications*, Royal Society of Chemistry, Cambridge, 2011.
23 R. Murugavel, A. Choudhury, M. G. Walawalkar, R. Pothiraja and C. N. R. Rao, *Chem. Rev.*, 2008, **108**, 3549.
24 G. P. Funkhouser, N. Tonmukayakul and F. Liang, *Langmuir*, 2009, **25**, 8672.
25 M. R. Mason, *J. Cluster. Sci.*, 1998, **9**, 1.
26 K. Maeda and F. Mizukami, *Catal. Surv. Jpn.*, 1999, **3**, 119.
27 C. G. Lugmair, T. D. Tilley and A. L. Rheingold, *Chem. Mater.*, 1999, **11**, 1615.
28 *US Pat.*, 4 929 589, 1990.
29 S. T. Meyers, J. T. Anderson, D. Hong, C. M. Hung, J. F. Wager and D. A. Keszler, *Chem. Mater.*, 2007, **19**, 4023.
30 R. N. Rothon, *Thin Solid Films*, 1981, **77**, 149.
31 Y. Huang, J. Ma, J. Yang, K. Cao and Z. Lu, *J. Phys. Chem. C*, 2012, **116**, 22518.
32 Y. Cao, Y. Ju, F. Liao, X. Jin, X. Dai, J. Li and X. Wang, *RSC Adv.*, 2016, **6**, 14852.
33 J. Ma, J. Yang, Y. Huang and K. Cao, *J. Mater. Chem.*, 2012, **22**, 2007.
34 X. Lin, S. Du, J. Long, L. Chen and Y. Wang, *ACS Appl. Mater. Interfaces*, 2016, **8**, 881.
35 H. Tanaka and M. Chikazawa, *Mater. Res. Bull.*, 2000, **35**, 75.
36 Z. Ding, B, Chen, J. Ding, L. Wang and Y. Han, *J. Colloid Interface Sci.*, 2014, **425**, 102.
37 R. Murugavel and S. Kuppuswamy, *Angew. Chem. Int. Ed.*, 2006, **45**, 1.
38 Z. Florjańczyk, A. Lasota, A. Wolak and J. Zachara, *Chem. Mater.*, 2006, **18**, 1995.
39 K. L. Fujdala and T. D. Tilley, *J. Am. Chem. Soc.*, 2001, **123**, 10133.
40 J. Pinkas, D. Chakraborty, Y. Yang, R. Murugavel, M. Noltemeyer and H. W. Roesky, *Organometallics*, 1999, **18**, 523.
41 R. Murugavel, M. G. Walawalkar, M. Dan, H. W. Roesky and C. N. R. Rao, *Acc. Chem. Res.*, 2004, **37**, 763.
42 M. Debowski, Z. Florjanczyk, K. Łokaj, A. Wolak, J. Zachara, M. Heneczkowski, M. Oleksy and H. Galina, presented in part at the 8th IUPAC International Conference on Novel Materials and their Synthesis (NMS-VIII) & 22nd International Symposium on Fine Chemistry and Functional Polymers (FCFP-XXII), Xi'An, China, October 14–19, 2012.
43 Z. Florjańczyk, A. Lasota and M. Leśniewska-Mizak, *Polimery*, 2004, **49**, 389.
44 *PL Pat.*, 197 233, 2008.
45 Z. Florjańczyk, A. Wolak, M. Dębowski, A. Plichta, J. Ryszkowska, J. Zachara, A. Ostrowski, E. Zawadzak and M. Jurczyk-Kowalska, *Chem. Mater.*, 2007, **19**, 5584.
46 Z. Florjańczyk, M. Dębowski, A. Wolak, M. Malesa and J. Płecha, *J. Appl. Polym. Sci.*, 2007, **105**, 80.
47 H. Fischer, *Mater. Sci. Eng.*, 2003, **C23**, 763.
48 B. Mossety-Leszczak, M. Włodarska, M. Kowalik and K. Łokaj, *Macromol. Symp.*, 2013, **329**, 193.
49 B. Mossety-Leszczak, B. Strachota, A. Strachota, M. Steinhart and M. Slouf, *Eur. Polym. J.*, 2015, **72**, 238.
50 TOPAS V.5, Bruker AXS, Karlsruhe, Germany, 2014.
51 Oxford Diffraction CRYSALIS^{PRO}, Oxford Diffraction Ltd., Abingdon, England, 2009.
52 G. M. Sheldrick, *Acta Crystallogr., Sect. A: Found. Crystallogr.*, 2008, **64**, 112.
53 I. D. Brown and D. Altermatt, *Acta Crystallogr., Sect. B: Struct. Sci.*, 1985, **41**, 244.
54 A. Aimi, D. Mori, K. Hiraki, T. Takahashi, Y. J. Shan, Y. Shirako, J. Zhou and Y. Inaguma, *Chem. Mater.*, 2014, **26**, 2601.
55 J. Zachara, *Inorg. Chem.*, 2007, **46**, 9760.
56 IUPAC Gold Book Home Page, http://goldbook.iupac.org/T06406.html (accessed December 21, 2015).
57 J. Florián, V. Baumruk, M. Štrajbl, L. Bednárová and J. Štěpánek, *J. Phys. Chem.*, 1996, **100**, 1559.
58 S. Beaucamp, D. Mathieu and V. Agafonov, *Acta Crystallogr., Sect. B: Struct. Sci.*, 2007, **63**, 277.
59 K. Maeda, Y. Kiyozumi and F. Mizukami, *Angew. Chem. Int. Ed. Engl.*, 1994, **33**, 2335.
60 K. Maeda, J. Akimoto, Y. Kiyozumi and F. Mizukami, *Angew. Chem. Int. Ed. Engl.*, 1995, **34**, 1199.
61 K. Maeda, J. Akimoto, Y. Kiyozumi and F. Mizukami, *J. Chem. Soc., Chem. Commun.*, 1995, 1033.
62 K. Maeda, Y. Hashiguchi, Y. Kiyozumi and F. Mizukami, *Bull. Chem. Soc. Jpn.*, 1997, **70**, 345.
63 D. Zhou, J. Xu, J. Yu, L. Chen, F. Deng and R. Xu,, *J. Phys. Chem. B*, 2006, **110**, 2131.
64 Y. Huang and Z. Yan, *J. Am. Chem. Soc.*, 2005, **127**, 2731.
65 M. R. Mason, R. M. Matthews, M. S. Mashuta and J. F. Richardson, *Inorg. Chem.*, 1996, **35**, 5756.
66 M. P. J. Peeters, J. W. de Haan, L. J. M. van de Ven and J. H. C. van Hooff, *J. Phys. Chem.*, 1993, **97**, 5363.
67 Y. Guan, G. S. –C. R. Glaser and G. J. Thomas Jr., *J. Phys. Chem.*, 1995, **99**, 12054.
68 Y. Guan and G. J. Thomas Jr., *Biopolymers*, 1996, **39**, 813.
69 B. Jayaram, M. Mezei and D. L. Beveridge, *J. Am. Chem. Soc.*, 1988, **110**, 1691.
70 *EP Pat.*, 2 628 766, 2014.
71 R. F. Mortlock, A. T. Bell and C. J. Radke, *J. Phys. Chem.*, 1993, **97**, 767.
72 R. F. Mortlock, A. T. Bell and C. J. Radke, *J. Phys. Chem.*, 1993, **97**, 775.

Table 1. Crystal and structure refinement data for DEPAl.

formula	$C_{12}H_{30}AlO_{12}P_3$
molecular weight [g mol^{-1}]	486.26
crystal system	trigonal
space group	$P\bar{3}$
a [Å]	20.43184(12)
b [Å]	20.43184(12)
c [Å]	8.99609(6)
α [°]	90
β [°]	90
γ [°]	120
cell volume [Å^3]	3252.36(3)
Z	6
ρ_{calcd} [g cm^{-3}]	1.490
crystal dimensions [mm]	0.08 × 0.10 × 0.32
measurement temperature [°C]	−173(2)
radiation λ [Å]	0.71073
μ [mm^{-1}]	0.370
θ_{min}–θ_{max} [°]	3.2–33.0
no. of measured reflections	101704
no. of unique reflections	7909
R_{int}	0.042
observed data [$I > 2\sigma(I)$]	7212
index ranges	$-30 \le h \le 30$
	$-30 \le k \le 31$
	$-13 \le l \le 13$
N_{ref}	7909
N_{par}	272
R_1 for observed data	0.0262
wR_2 for observed data	0.0717
goodness-of-fit	1.031
residual density: min/max [e Å^{-3}]	−0.34/0.55

Table 2. Elemental analysis of DBPAl, BEHPAl and DPhPAl samples synthesized by different methods.

DOPAl	DOPAl formula (theoretical values)[a]	Results of elemental analysis		
		Method of synthesis[b]	C [%]	H [%]
DBPAl	$C_{24}H_{54}AlO_{12}P_3$	TOP (M2)	43.72	8.08
	(C, 44.04; H, 8.32%)	DOP (M1)	43.82	8.29
		DOPNa	43.51	8.21
		DOP-TEA	43.87	8.49
BEHPAl	$C_{48}H_{102}AlO_{12}P_3$	DOP (M2)	56.53	10.11
	(C, 58.16; H, 10.37%)	DOPNa	57.14	10.25
		DOP-TEA	57.41	10.59
DPhPAl	$C_{36}H_{30}AlO_{12}P_3$	TOP (M2)	55.67	4.03
	(C, 55.83; H, 3.90%)	TOP (M3)	54.14	4.12
		DOP (M3)	55.61[c]	3.93[c]
			55.42[d]	4.07[d]
		DOPNa	54.79	4.07

[a] values of carbon and hydrogen content calculated for the assumed DOPAl formula. [b] TOP, DOP, DOPNa, DOP-TEA – synthetic routes; M1, M2 and M3 – method of synthesis within the respective synthetic route. [c] reaction time 1 h. [d] reaction time 24 h.

Table 3. Octahedral distortions (Δ_{Al}), O–Al–O angle variances (σ^2), bond valence sums (s_{Al}), and length of the resultant bond-valence vector ($|\mathbf{v}_{Al}|$) for each crystallographically independent aluminum coordination center in DEPAl.

Atom	$\Delta_{Al}\times10^5$	σ^2 [(°)^2]	s_{Al}[a]	$\lvert\mathbf{v}_{Al}\rvert$ [v.u][b]
Al1	0	1.5	3.05	0.000
Al2	0	2.0	3.02	0.000
Al11	0.11	1.0	3.06	0.003
Al12	0.03	1.1	2.97	0.003

[a] Bond valences were calculated according to the method proposed in the literature[42] (for details, see ESI†). [b] valence units.

Table 4. Bond valence sums (s_P) and length of the resultant bond-valence vector ($|\mathbf{v}_P|$) for each crystallographically independent phosphorus coordination center in DEPAl.

Atom	s_P[a]	$\lvert\mathbf{v}_P\rvert$ [v.u.][b]
P1	4.98	0.003
P11	4.97	0.074
P12	4.98	0.077

[a] Bond valences were calculated according to the method proposed in the literature[42] (for details, see ESI†). [b] valence units.

Table 5. The main peak position in PXRD diffractograms measured at room temperature (2θ), the corresponding interplanar distance ($d_{2\theta}$), and monomeric unit volumes evaluated for different DOPAl samples.

DOPAl	2θ [°]	$d_{2\theta}$ [Å]	V_{calcd} [Å^3]	V_{XRD} [Å^3]	ΔV [%][a]
DMPAl	9.68	9.13	429	443	3.3
DEPAl	8.47	10.44	575	578	0.5
DnPPAl	7.52	11.75	722	734	1.7
DiPPAl	7.76	11.38	738	688	−6.8
DBPAl	6.64	13.31	868	941	8.4
BEHPAl	5.35	16.50	1471	1445	−1.8
DPhPAl	6.73	13.12	898	915	1.9

[a] $\Delta V = 100 \times (V_{XRD} - V_{calcd})/V_{calcd}$.

Table 6. Relative integral intensities of signals observed in ^{1}H or ^{31}P NMR spectra of DMPAl aqueous solutions and the content of the corresponding dimethylphosphate groups.

Solution	δ_P [ppm]	Relative integral	mol%	δ_H [ppm]	Relative integral	mol%
saturated	5.82	10.17	59	3.58	6.60	57
	−3.47	6.09	35	3.65	4.03	35
	−8.79	1.00	6	3.75	1.00	8
dilute	5.87	2.50	71	3.59	26.82	69
	−3.43	1.00	29	3.68	11.25	29
	–	–	–	3.77	1.00	2

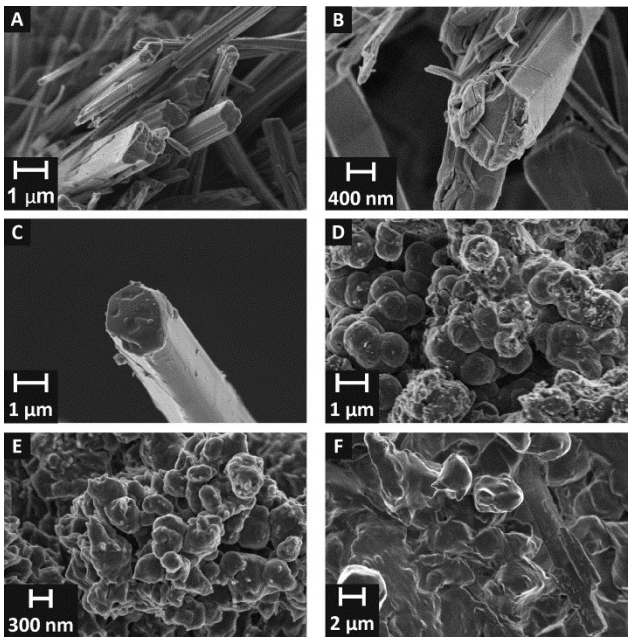

Fig. 1 SEM images of DMPAl (A), DnPPAl (B), DBPAl (C, D), and BEHPAl (E, F). The products were synthesized from AlLact and the appropriate amount of TOP (images A–C), DOP (images D–E), or DOPNa (F).

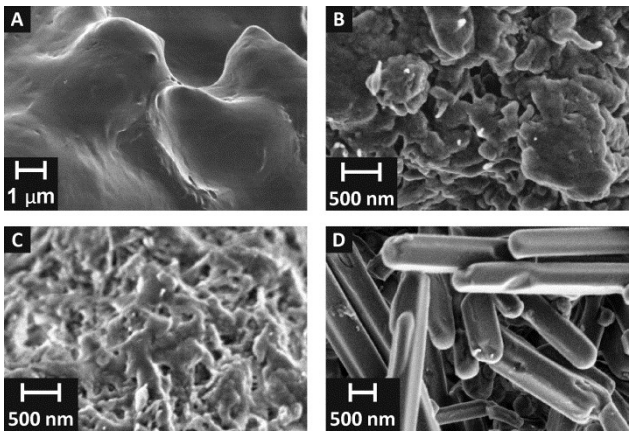

Fig. 2 SEM images of BEHPAl (A) and DBPAl (B–D) synthesized from TEA and DOP. For DBPAl: the as-synthesized product (B), the product heated in toluene for 12 h (C), and the product heated with 1-butanol/water mixture (40:60 v/v) (D).

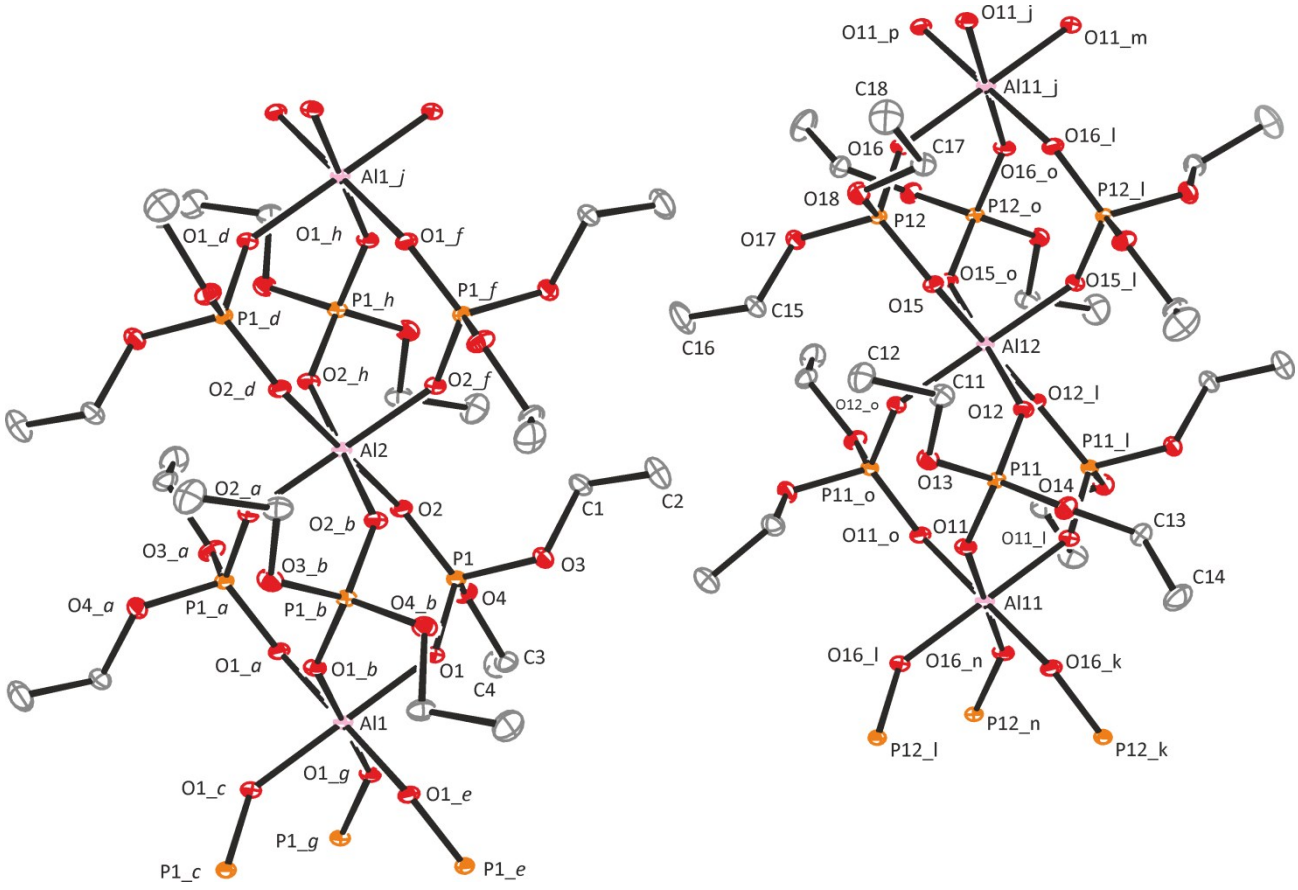

Fig. 3 ORTEP diagram of DEPAl crystal structure with an *A*-type chain on the left side and a *B*-type chain on the right side. *a*–*p* are the symbols of translation symmetry for equivalent positions defined in Table S1.

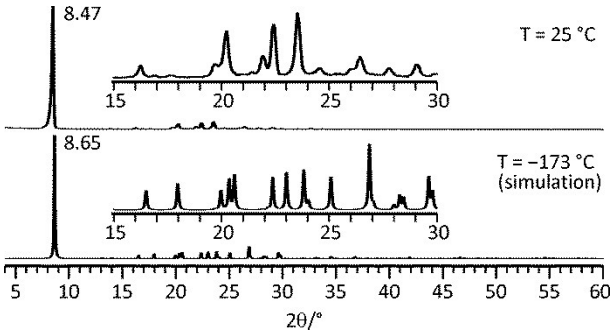

Fig. 4 PXRD patterns of DEPAl measured at room temperature and calculated from the data obtained in single–crystal X-ray analysis carried out at −173 °C.

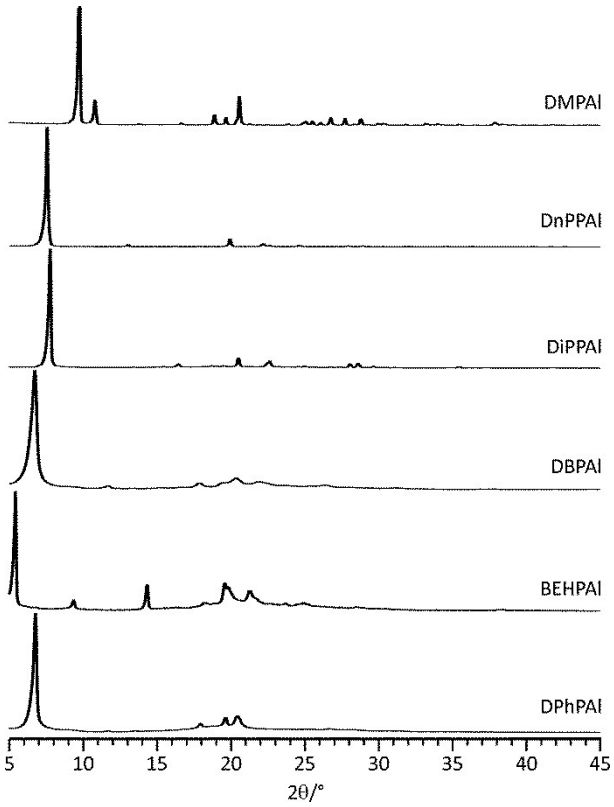

Fig. 5 PXRD patterns for different DOPAl samples measured at room temperature.

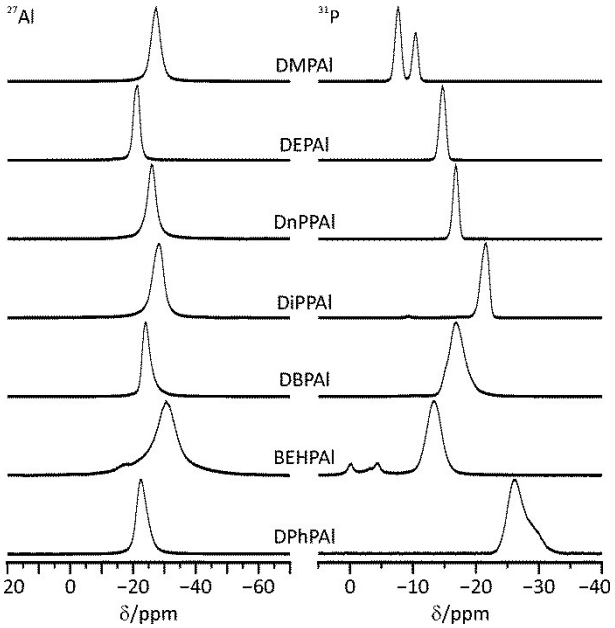

Fig. 6 ^{27}Al (left) and ^{31}P (right) MAS NMR spectra of DOPAl recorded at room temperature.

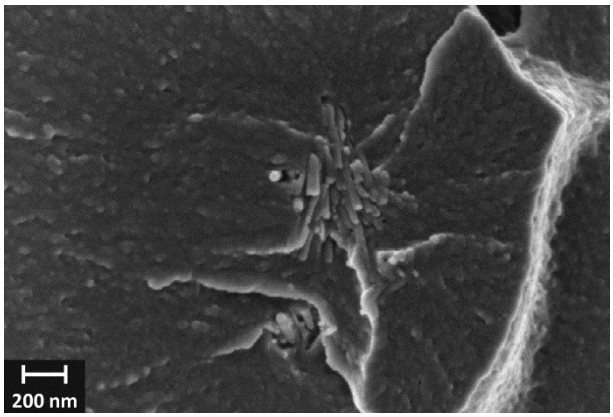

Fig. 7 SEM image of an epoxy resin cured with a solution of DPhPAl in triethylenetetramine.

The synthesis and properties of coordination polymers with formula $Al[O_2P(OR)_2]_3$ [R= Me, Et, ^{n}Pr, ^{i}Pr, ^{n}Bu, $CH_2CH(Et)(CH_2)_3CH_3$ or Ph] are reported.